# A NUMERICAL STUDY FOR THE PERFORMANCE OF THE WENO SCHEMES BASED ON DIFFERENT NUMERICAL FLUXES FOR THE SHALLOW WATER EQUATIONS [*]

Changna Lu

*College of Mathematics and Physics, Nanjing University of Information Science and Technology, Nanjing 210044, China*

*E-mail:luchangna@163.com*

Jianxian Qiu

*Department of Mathematics, Nanjing University, Nanjing 210093, China*

*E-mail: jxqiu@nju.edu.cn*

Ruyun Wang

*College of Ocean, Hohai University, Nanjing, Jiangsu 210098, P.R. China*

*E-mail: wangruyun@163.com*

## Abstract

In this paper we investigate the performance of the weighted essential non-oscillatory (WENO) methods based on different numerical fluxes, with the objective of obtaining better performance for the shallow water equations by choosing suitable numerical fluxes. We consider six numerical fluxes, i.e., Lax-Friedrichs, local Lax-Friedrichs, Engquist-Osher, Harten-Lax-van Leer, HLLC and the first-order centered fluxes, with the WENO finite volume method and TVD Runge-Kutta time discretization for the shallow water equations. The detailed numerical study is performed for both one-dimensional and two-dimensional shallow water equations by addressing the issues of CPU cost, accuracy, non-oscillatory property, and resolution of discontinuities.

*Mathematics subject classification:* 65M60, 65M99, 35L65.
*Key words:* Numerical flux, WENO finite volume scheme, Shallow water equations, High order accuracy, Approximate Riemann solver, Runge-Kutta time discretization.

## 1. Introduction

In this paper, we investigate the performance of the WENO methods based on different numerical fluxes for the shallow water equations, with the objective of obtaining better performance by choosing suitable numerical fluxes. The weighted essential non-oscillatory (WENO) scheme [10,14] is a procedure of spatial discretization; namely, it is a procedure to approximate the spatial derivative terms. The WENO scheme uses the idea of adaptive stencils in the reconstruction procedure based on the local smoothness of the numerical solution to automatically achieve high order accuracy and a non-oscillatory property near discontinuities. The WENO method has been developed in recent years as a class of high order method for the shallow water equations [3,5,26,27], which gives sharp, non-oscillatory discontinuity transitions and at the same time provides high order accurate resolutions for the smooth part of the solution. The WENO schemes are widely studied after the structure of the finite difference WENO schemes were proposed from the ENO schemes by Jiang and Shu in 1996 [10]. The construction of finite

volume WENO methods on unstructured meshes was presented by Friedrichs [6]. Instead of constructing two-dimensional finite volume WENO schemes with dimensional by dimensional methods, Hu and Shu [9] proposed a full dimensional reconstruction methodology for the third order WENO schemes by using a combination of two-dimensional linear polynomials and the third and fourth order WENO schemes by using a combination of two-dimensional quadratic polynomials. Then the WENO schemes were used in the shallow water flows simulations. Xing and Shu [27] developed a treatment for the bed slope source term of the shallow water equations using the fifth-order finite difference WENO scheme. In [26], Vukovic and Sopta used the finite difference ENO and WENO to solve the one-dimensional shallow water flows in order to maintain genuine high-order accuracy. Both finite volume WENO and central WENO schemes were used in [5] to solve the shallow water equations; high accuracy and well balancing are obtained in the paper.

An important component of the WENO methods for the shallow water equations is the numerical flux based on exact or approximate Riemann solvers. In most of the WENO methods, Lax-Friedrichs (LF) numerical flux is used due to its simplicity. However, there exist many other numerical fluxes based on exact or approximate Riemann solvers documented in the book of Toro [23,24], which could also be used in the context of the WENO method. The high-order accurate WENO schemes and the HLLC approximate Riemann solver are used in compressible multicomponent flow problems [11]. A comparison is made between the difference schemes of Engquist, Fisher, and Roe fluxes with Galerkin methods for approximating hyperbolic conservation laws [16]. The Godunov flux [7,23,24] is based on exact Riemann solver, which has the smallest viscosity among all the monotone numerical fluxes, but it often lacks explicit formulas and relies on iterative procedures. In this paper, we will consider six numerical fluxes except the Godunov flux based on approximate Riemann solvers, which are LF flux, local LF (LLF) flux, EO flux, Harten-Lax-van Leer (HLL) flux, HLLC flux, the first-order centered (Force) flux, and compare the performance of the WENO methods based on these numerical fluxes for the shallow water equations, with the objective of obtaining better performance by choosing suitable numerical fluxes. We review and describe the details of the numerical fluxes under consideration in section 2, and present extensive numerical tests in section 3 to compare their performance for the shallow water equations. The detailed numerical study is performed for the one-dimensional and two-dimensional shallow water equations. Concluding remarks are given in section 4.

## 2. Review and Implementation of the Numerical Fluxes for the WENO Method

In this section, we review the WENO method for the shallow water equations and the numerical fluxes under consideration of the WENO method. We mainly describe the WENO method for the one-dimensional case. Consider the one-dimensional shallow water equations:

$$U_t + F(U)_x = S(U), \tag{2.1}$$

with

$$U = [h, hu]^T, \ \ F(U) = [hu, hu^2 + \frac{1}{2}gh^2]^T, \ \ S = [0, -ghb_x]^T,$$

where $U$ is the vector of conservative variables, $F$ is the flux vector, $S$ is the source term relative to the bottom slope, $t$ is the time, $x$ is the space, $h$ is the water height, $u$ is the vertically averaged velocity, $g$ is the gravity, and $b$ is the bottom elevation.

Spatial discretization of the computational domain is based on a spatial step $\Delta x$, a uniformly spaced mesh defined by $x_i = (i + \frac{1}{2})\Delta x$. Denote $I_i = [x_{i-\frac{1}{2}}, x_{i+\frac{1}{2}}]$ be the *ith* cell, centered on $x_i$. The updating conservative formula for (2.1) is

$$\frac{d}{dt}\bar{U}_i + \frac{1}{\Delta x}[\hat{F}(U_{i+\frac{1}{2},L}, U_{i+\frac{1}{2},R}) - \hat{F}(U_{i-\frac{1}{2},L}, U_{i-\frac{1}{2},R})] = \bar{S}_i, \tag{2.2}$$

where $U_{i+\frac{1}{2},L}$, $U_{i+\frac{1}{2},R}$ are the left and the right reconstructions of the discontinuous solution at the cell interface $x_{i+\frac{1}{2}}$; $\hat{F}(U_L, U_R)$ is the numerical flux based on exact or approximate Riemann solvers, which will be mainly discussed in this paper; $\bar{U}_i$, $\bar{S}_i$ are the cell-averaged terms. The semi-discrete scheme (2.2) is discretized in time by the third order nonlinear stable Runge-Kutta time discretization. The fifth order WENO finite volume scheme is used for the reconstruction for one-dimensional cases, and the third order is used for two-dimensional cases. The details of the WENO on unstructured meshes can be found in [9].

We now review the numerical fluxes under consideration, and the comparison of their performance will be given in the next section.

### 2.1. The Lax-Friedrichs (LF) flux and the local LF (LLF) flux [13, 18, 23]

The LF flux is one of the simplest and most widely used. However, the numerical viscosity of the LF flux is also the largest among monotone numerical fluxes. The LF or the LLF is defined by:

$$\hat{F}^{LF}(U_L, U_R) = \frac{1}{2}\left(F(U_L) + F(U_R) - \alpha(U_R - U_L)\right), \tag{2.3}$$

where for the LF flux, $\alpha$ is taken as an upper bound over the whole line for $|F'(U)|$ in the scalar case, or for the absolute value of eigenvalues of the Jacobian for the system case, and for the LLF flux $\alpha$ is taken as an upper bound between $U_L$ and $U_R$.

### 2.2. The Engquist-Osher (EO) flux and the Osher-Solomon flux [13, 24]

The EO flux for the scalar case and its extension to systems (often referred to as the Osher-Solomon flux) are based on the approximate Riemann solvers; they have the advantage of explicit formulas for the scalar case and many systems. For given initial data $U_L$ and $U_R$, it is conventional in the EO scheme to define: $U_0 = U_L$, $U_1 = U_R$. The intersection points $U_{\frac{1}{3}}$ and $U_{\frac{2}{3}}$ are found to be:

$$h_{\frac{1}{3}} = \left(\frac{1}{2}(a_L + a_R) - \frac{1}{4}(u_R - u_L)\right)^2 / g, \quad u_{\frac{1}{3}} = \frac{1}{2}(u_L + u_R) + a_L - a_R, \quad v_{\frac{1}{3}} = v_0;$$

$$h_{\frac{2}{3}} = \left(\frac{1}{2}(a_L + a_R - \frac{1}{4}(u_R - u_L)\right)^2 / g, \quad u_{\frac{2}{3}} = \frac{1}{2}t(u_L + u_R + a_L - a_R), \quad v_{\frac{2}{3}} = v_1.$$

with $a = \sqrt{gh}$. The sonic points are found to be:

$$u_{S0} = \frac{1}{3}(u_0 + 2a_0), \quad a_{S0} = u_{S0}, \quad h_{S0} = a_{S0}^2/g, \quad v_{S0} = v_0;$$

$$u_{S1} = \frac{1}{3}(u_1 - 2a_1), \quad a_{S1} = -u_{S1}, \quad h_{S1} = a_{S1}^2/g, \quad v_{S1} = v_1.$$

To compute the numerical flux using the EO Riemann solver for the shallow water equations, one must form the flux as the summation of all the partial fluxes in the appropriate entry of Table 2.1, where a total of 16 cases need to take care of, with $u_* = \frac{1}{2}(u_L + u_R) + a_L - a_R$.

Table 2.1: The Engquist-Osher flux formula for the shallow water equations, with $F_K \equiv F(U_K)$.

| | $u_0 - a_0 \geq 0$ $u_1 + a_1 \geq 0$ | $u_0 - a_0 \geq 0$ $u_1 + a_1 \leq 0$ | $u_0 - a_0 \leq 0$ $u_1 + a_1 \geq 0$ | $u_0 - a_0 \leq 0$ $u_1 + a_1 \leq 0$ |
|---|---|---|---|---|
| $u_* \geq 0, u_* - a_{\frac{1}{3}} \geq 0$ | $F_0$ | $F_0 + F_1 - F_{S1}$ | $F_{S0}$ | $F_{S0} - F_{S1} + F_1$ |
| $u_* \geq 0, u_* - a_{\frac{1}{3}} \leq 0$ | $F_0 - F_{S0} + F_{\frac{1}{3}}$ | $F_0 - F_{S0} + F_{\frac{1}{3}} - F_{S1} + F_1$ | $F_{\frac{1}{3}}$ | $F_1 + F_{\frac{1}{3}} - F_{S1}$ |
| $u_* \leq 0, u_* + a_{\frac{2}{3}} \geq 0$ | $F_0 - F_{S0} + F_{\frac{2}{3}}$ | $F_0 - F_{S0} + F_{\frac{2}{3}} - F_{S1} + F_1$ | $F_{\frac{2}{3}}$ | $F_1 + F_{\frac{2}{3}} - F_{S1}$ |
| $u_* \leq 0, u_* + a_{\frac{2}{3}} \leq 0$ | $F_0 - F_{S0} + F_{S1}$ | $F_0 - F_{S0} + F_1$ | $F_{S1}$ | $F_1$ |

## 2.3. The Harten-Lax-van Leer (HLL) flux [23–25]

The HLL flux is based on the approximate Riemann solver with three constant states separated by two waves. The evaluation of the HLL flux is simple and fast, however it has the shortcoming of poor resolution for contact discontinuities, shear waves and material interfaces. The HLL flux for the shallow water equations is given by:

$$
\hat{F}^{HLL}(U_L, U_R) = \begin{cases} F(U_L) & s_L \geq 0 \\ \dfrac{s_R F(U_L) - s_L F(U_R) + s_R s_L (U_R - U_L)}{s_R - s_L} & s_L \leq 0 \leq s_R \\ F(U_R) & s_R \geq 0 \end{cases} , \qquad (2.4)
$$

where the lower and upper bounds of the speed, $s_L$ and $s_R$, have several possible choices available. The following choice of wave speed estimates leads to accuracy and robust scheme:

$$
s_L = u_L - a_L q_L, \quad s_R = u_R - a_R q_R, \qquad (2.5)
$$

where $q_K(K = L, R)$ is given by:

$$
q_K = \begin{cases} \sqrt{\dfrac{1}{2}\big[\dfrac{(h_* + h_K)h_*}{h_K^2}\big]} & h_* \geq h_K \\ 1 & h_* < h_K \end{cases} , \qquad (2.6)
$$

with

$$
h_* = \frac{1}{g}\left(\frac{1}{2}(a_L + a_R) + \frac{1}{4}(u_L - u_R)\right)^2 . \qquad (2.7)
$$

## 2.4. The HLLC flux—a modification of the HLL flux [2, 8, 24]

The HLLC flux based on the approximate Riemann solver is a modification to account for the shortcoming of the HLL flux, offset the influence of intermediate waves. In addition to the wave speed estimates $s_L$ and $s_R$ in the HLL solver, an estimate $s_*$ for the speed of the middle wave is need. The HLLC flux for the shallow water equations is given by:

$$
\hat{F}^{HLLC}(U_L, U_R) = \begin{cases} F(U_L) & s_L \geq 0, \\ F(U_L) + s_L(U_{*L} - U_L) & s_L \leq 0 \leq s_*, \\ F(U_R) + s_R(U_{*R} - U_R) & s_* \leq 0 \leq s_R, \\ F(U_R) & s_R \leq 0, \end{cases} \qquad (2.8)
$$

where

$$
U_{*K} = h_K\left(\frac{s_K - u_K}{s_K - s_*}\right)\begin{pmatrix} 1 \\ s_* \\ v_K \end{pmatrix}, \quad s_* = \frac{s_L h_R(u_R - s_R) - s_R h_L(u_L - s_L)}{h_R(u_R - s_R) - h_L(u_L - s_L)}, \qquad (2.9)
$$

and the definitions of $s_L$ and $s_R$ are given in (2.5).

### 2.5. The first-order centered (FORCE) flux [23, 24]

The FORCE flux is given by:

$$\hat{F}^{FORCE}(U_L, U_R) = \frac{1}{2}\big(\hat{F}^{LF}(U_L, U_R) + \hat{F}^{LW2}(U_L, U_R)\big), \tag{2.10}$$

where $\hat{F}^{LF}(U_L, U_R)$ is the LF flux and $\hat{F}^{LW2}(U_L, U_R)$ is the Richemyer or two-step Lax-Wendroff flux, i.e.,

$$\hat{F}^{LW2}(U_L, U_R) = F(U^{LW2}), \tag{2.11}$$

with

$$U^{LW2} = \frac{1}{2}\left(U_L + U_R + \frac{\Delta t}{\Delta x}(F(U_L) - F(U_R))\right). \tag{2.12}$$

The FORCE flux is the average of the LF flux and the Lax-Wendroff flux; hence its viscosity is smaller than that of the LF flux.

## 3. Numerical Results

In this section, we make extensive numerical tests to compare the performance of the WENO finite volume methods based on the six numerical fluxes outlined in the previous section. The detailed numerical study is mainly performed for the one-dimensional system case, addressing the issues of CPU cost, accuracy, non-oscillatory property, and resolution of discontinuities. Numerical tests are also performed for the two-dimensional systems.

For non-flat bed shallow flows, we adopt the ideas of Rogers et al. [20], who presented an algebraic technique for balancing flux gradients and source terms. We describe it in one-dimensional case simply. The vector of conserved variables $U$ is given by

$$U = U^{eq} + U',$$

where $U'$ is the deviation of $U$ from the equilibrium or still water value such that $\partial U^{eq}/\partial t = 0$. Actually, for still water values, the shallow water convenient properties are $\zeta = u = 0$, and

$$U^{eq} = [D, 0]^T, \quad U' = U - U^{eq} = [\zeta, uh]^T, \tag{3.1}$$

where $\zeta$ is the free water height above the still water level $D$, $h = \zeta + D$ is the total water depth. The approach taken in the paper is to use the still water level as the datum $D$. It is perfectly reasonable to choose a fixed horizontal datum elsewhere and derive the balanced hyperbolic equations using a stage-discharge approach.

The shallow water equations are transformed to

$$U_t' + F'(U)_x = S', \tag{3.2}$$

with

$$U' = [\zeta, uh]^T, \quad F' = [uh, (hu)^2/(\zeta + D) + g(\zeta^2 + 2D\zeta)/2]^T, \quad S' = [0, -g\zeta b_x]^T. \tag{3.3}$$

We can see that the Jacobian and the discretization of (3.2) is the same as that of (2.1).

For CPU time comparison, all the computations are performed on a personal computer, Core (TM) 2 CPU 4400 @ 2.00 GHz with 512 MB ram. We denote the WENO scheme with the numerical flux "X" as WENO-X, such as WENO-LF for the WENO scheme with the LF flux. In our numerical experiments, we use the fifth-order WENO scheme for one-dimensional cases, and the third-order for two-dimensional cases on unstructure (triangle) meshes. The CFL number is taken as 0.6, the gravitation constant is taken as $9.812 m/s^2$, the small positive constant in the WENO weight formula is taken as $\varepsilon = 10^{-6}$, except for the small pulse problem.

**Example 3.1.**

An accuracy test over a sinusoidal hump [3, 27]. The bottom elevation is described by the following function:

$$b(x) = \sin^2(\pi x), \quad x \in [0, 1], \tag{3.4}$$

with initial conditions:

$$h(x, 0) = 5 + e^{\cos(2\pi x)}, \quad hu(x, 0) = \sin(\cos(2\pi x)). \tag{3.5}$$

Periodic boundary conditions are assumed. We take the still level $D$ as $D(x) = 5 - b(x)$. We compute up to $t = 0.1$ when the solution is still smooth. This test case can not be solved analytically and therefore a numerical solution computed by the WENO-LF on a mesh with 25,600 cells is adopted as the reference solution.
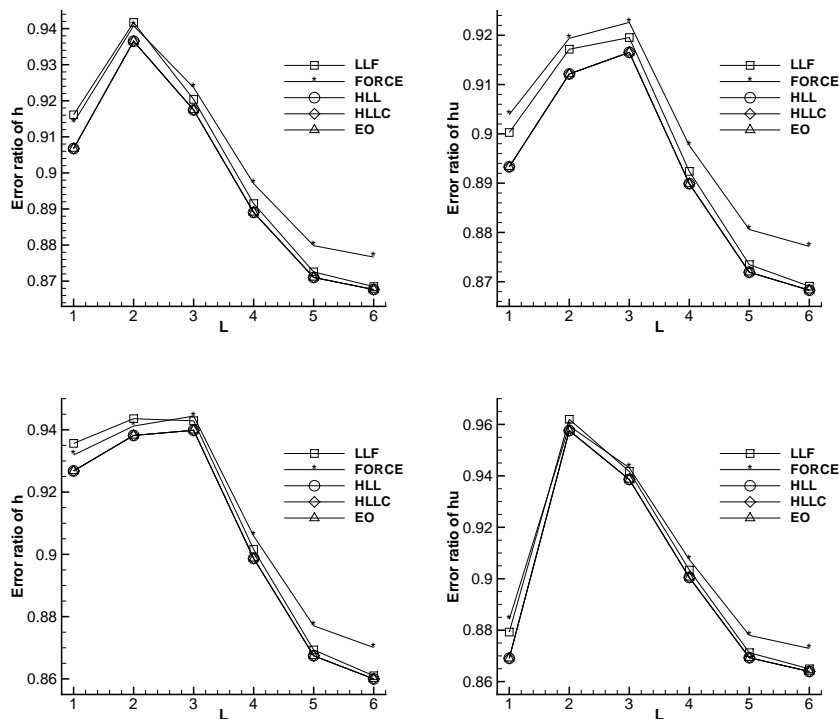


Fig. 3.1. An accuracy test over a sinusoidal hump. Error ratio of the $L_1$ numerical error for $h$ (top left) and $hu$ (top right) and of the $L_\infty$ numerical error for $h$ (bottom left) and $hu$ (bottom right) by the WENO methods based on different fluxes to that by the WENO-LF method on meshes with $N = 25 \cdot 2^{L-1}, (L = 1, 2, ...6)$ cells.
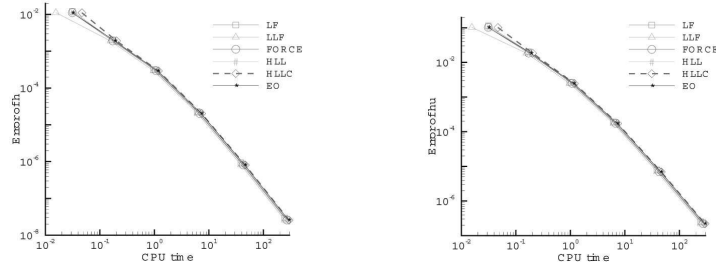
Fig. 3.2. An accuracy test over a sinusoidal hump. The $L_1$ numerical error and the CPU time (unit: second) using the log scale for $h$ (left) and $hu$ (right) by the WENO methods based on different fluxes on meshes with $N = 25 \cdot 2^{L-1}, (L = 1, 2, ...6)$ cells .

Table 3.1: An accuracy test over a sinusoidal hump. CPU time on meshes with $N$ cells using the WENO methods based on different fluxes (unit: second).

| $N$ | LF | LLF | FORCE | HLL | HLLC | EO |
|-----|------|------|--------|--------|--------|--------|
| 200 | 6.13 | 6.18 | 6.77 | 7.30 | 7.38 | 7.17 |
| 400 | 38.73 | 39.02 | 42.67 | 46.10 | 46.50 | 45.30 |
| 800 | 245.81 | 247.42 | 271.22 | 291.53 | 294.67 | 287.44 |

    To demonstrate the performance of these numerical fluxes, we show the error ratio of the $L_1$ and $L_\infty$ numerical error to that of the WENO-LF scheme in Figure 3.1 for different meshes, where the cell number is $N = 25 \cdot 2^{L-1}$, $L = 1, \cdots, 6$. The comparison of CPU time is shown in Table 3.1. We also show the $L_1$ numerical errors against the CPU time in Figure 3.2 for WENO schemes with different fluxes on different meshes.

    On the numerical errors, the errors by all the other schemes are about 85-95% of that by the WENO-LF scheme for all the meshes concerned, and the performance of the WENO-HLLC scheme is almost the same as that of the WENO-HLL and WENO-EO schemes, followed by the WENO-FORCE and the WENO-LLF schemes, then the WENO-LF scheme; the error ratio of the WENO-LLF scheme is better than that of the WENO-FORCE scheme when the mesh is refined after $N = 25 \cdot 2^{3-1}$. All schemes achieve their designed orders of accuracy, as expected, which are not shown here.

    On the CPU time, in Table 3.1 we can see that the WENO-LF method costs the least CPU time, the WENO-LLF, WENO-FORCE schemes cost a little more than that of the WENO-LF scheme. The WENO-EO, WENO-HLL, WENO-HLLC schemes cost about 20% more than that of the WENO-LF scheme, and the WENO-EO scheme costs the least hereinto. While the distinction of the $L_1$ numerical error against the CPU time for different fluxes is not so clear in Figure 3.2 except for $N = 25$. Of course, the CPU time comparison depends on our specific implementation of these fluxes and also on the specific test case, but it does give the correct ball-park of the relative CPU costs of the WENO methods using these different numerical fluxes for the shallow water equations.

**Example 3.2.** Dam break on a flat bed. The dam-break problem is the most common test to

evaluate the performance of shock capturing schemes in shallow flows, such as [15]. The bottom is flat $b(x) = 0$ and the initial conditions are taken as:

$$h(x, 0) = \begin{cases} h_1 & x < 0, \\ h_2 & x \geq 0, \end{cases} \quad hu(x, 0) = 0. \tag{3.6}$$

We take the computational domain as $[-1, 1]$, $h_1 = 1m$ and $h_2 = 0.1m$. The simulation is performed up to time $t = 0.1s$.
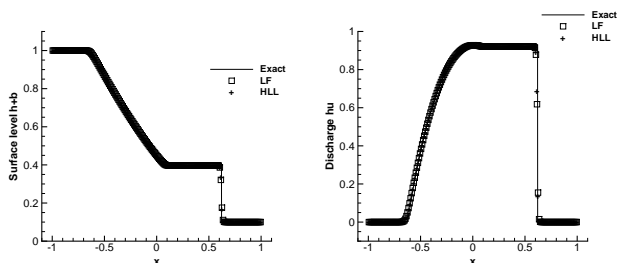
The surface level $h$ and the discharge $hu$ using the WENO schemes with different numerical fluxes on a mesh with 200 uniform cells are plotted in Figure **??**, which show very good agreement with the exact solution in [22]. In order to compare the quality of different numerical fluxes, we also show the $L_1$ numerical errors against the CPU time in Figure 3.4 for different numerical fluxes on different meshes, we run 10 times for every program as the CPU time. We can see from the figure that the line of the WENO-FORCE scheme almost keep lower side in this case, followed by that of the WENO-LLF scheme. The WENO-LF scheme keeps the upper side, which means that the WENO-LF scheme costs the most CPU time among all at the same error level.
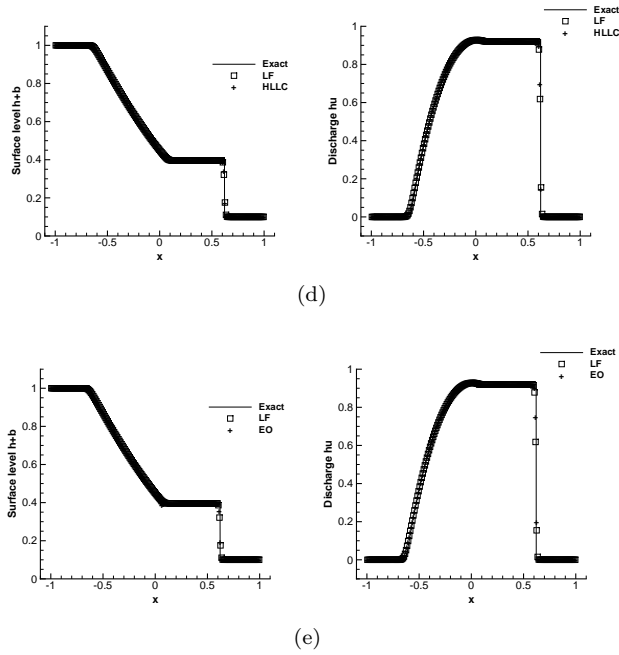


(a)



(b)



(c)

(d)



(e)
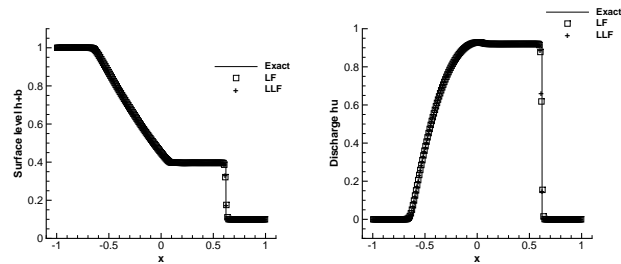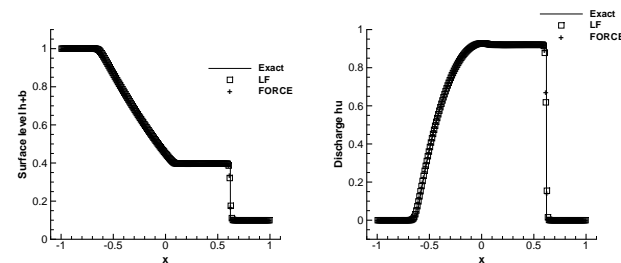
Fig. 3.3. Dam break on a flat bed at t = 0.1s. Left: the surface level h+b; Right: the discharge hu. Solid lines: the exact solution; hollow square: the results computed by the WENO-LF scheme; plus symbols: results computed by the (a)WENO-LLF, (b)WENO-FORCE, (c)WENO-HLL, (d)WENO-HLLC, and (e)WENO-EO.
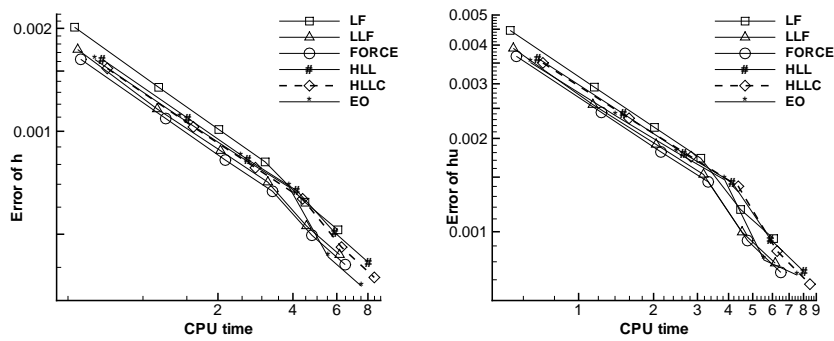


Fig. 3.4. Dam break on a flat bed. The $L_1$ numerical error and the CPU time (unit: second) using the log scale for $h$ (left) and $hu$ (right) by the WENO methods based on different fluxes on meshes with $N = 200, 300, 400, 500, 600, 700$ cells .

The bottom elevation is described by the following function:

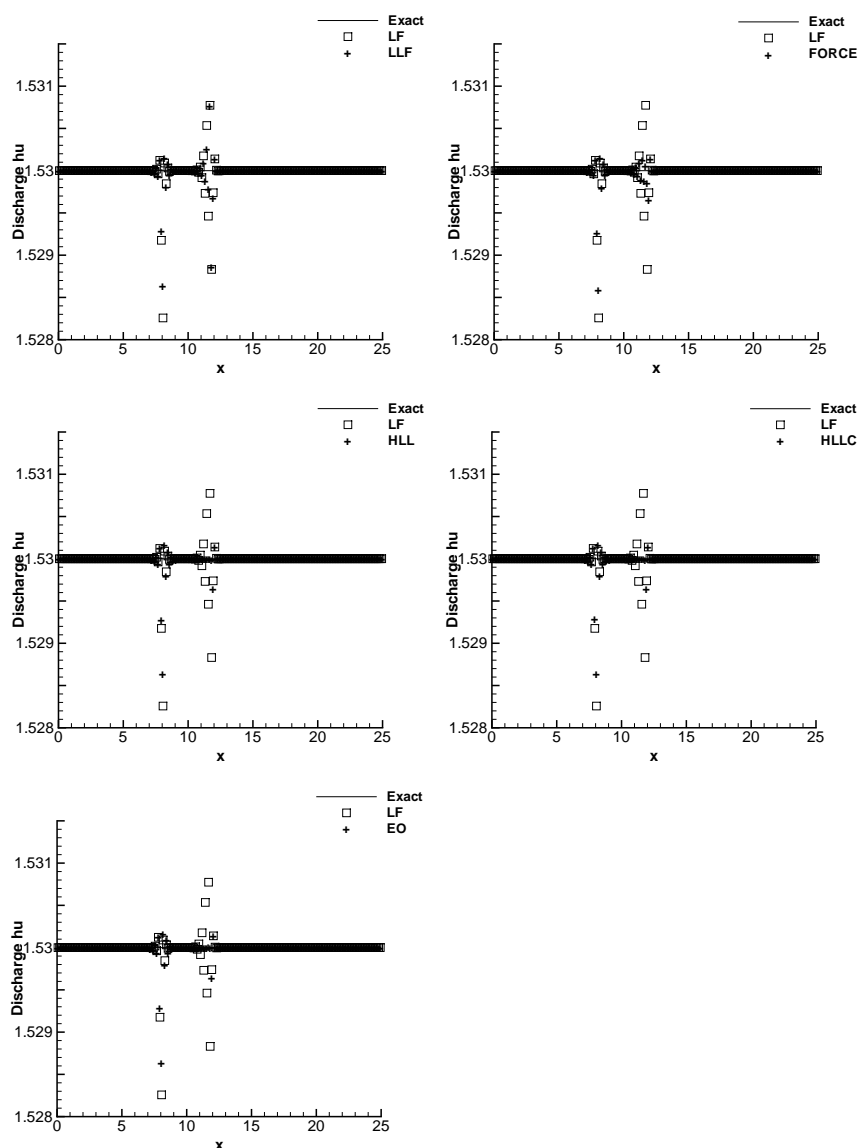$$b(x) = \begin{cases} 0.2 - 0.05(x - 10)^2 & 8 \leq x \leq 12, \\ 0 & \text{otherwise}, \end{cases} \qquad (3.7)$$

Fig. 3.5. Steady trans-critical flow over a hump without a shock. The discharge $hu$. Solid lines: the exact solution; hollow square: the results computed by the WENO-LF scheme; plus symbols: results computed by the WENO-LLF (top left), WENO-FORCE (top right), WENO-HLL (middle left), WENO-HLLC (middle right), and WENO-EO (bottom).

where $x \in [0, 25]$. The initial conditions are taken as:

$$h(x, 0) = 0.5 - b(x), \quad hu(x, 0) = 0. \tag{3.8}$$

**Example 3.3.** Steady discontinuous flow over a parabolic hump. The purpose of the test is to study the convergence in time towards steady flows on non-flat bed involving trans-critical and sub-critical flows; it is widely used to test numerical schemes for the shallow water equations, such as [3, 19, 27].
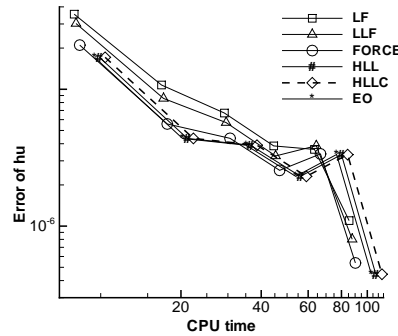
Fig. 3.6. Steady trans-critical flow over a hump without a shock. The $L_1$ numerical error (left) and the $L_\infty$ numerical error for $hu$ and the CPU time (unit: second) using the log scale by the WENO methods based on different numerical fluxes on meshes with $N = 200, 300, 400, 500, 600, 700$ cells .

Different steady solutions can be computed involving fully sub-critical and smooth trans-critical flow and trans-critical flow with a shock. We simulate the problem until time $t = 200s$ with two boundary conditions. We take the still level $D$ as $D(x) = 0.5 - b(x)$.

**(a)** Trans-critical flow without a shock.

Upstream: The discharge $hu = 1.53m^3/s$ is imposed. Downstream: The water height $h = 0.66m$ is imposed when the flow is sub-critical.

This is a transition from sub-critical to trans-critical. As the computed results of surface level $h + b$ by the WENO schemes with different fluxes are similar and comparable to the analysis, we do not show them to save space. In Figures 3.5, the computed discharge $hu$ (which should be constant and equal to 1.53 everywhere) are plotted against the numerical solution computed by the WENO-LF scheme on a mesh with 200 uniform cells. We can see that the result computed by the WENO-LF is the worst, and the results by WENO-EO, WENO-HLL and WENO-HLLC are comparable and better than that by WENO-LLF. The $L_1$ numerical errors against the CPU time of different fluxes for different meshes are displayed in Figure 3.6. We can see that the two lines of the WENO-LF scheme and the WENO-LLF scheme are above that of others almost everywhere, it also means that the WENO-LF scheme and the WENO-LLF scheme cost the more CPU time than the others at the same error level, hence the WENO-LF scheme and the WENO-LLF are less efficient than the others.

**(b)** Sub-critical flow with a shock.

Upstream: The discharge $hu = 4.42m^3/s$ is imposed. Downstream: The water height $h = 2m$ is imposed. The imposed conditions and the bottom elevation cause the purely sub-critical flow over the whole domain.

The comparison of the discharge (which should be constant and equal to 4.42 everywhere) using the WENO-LF scheme with the other schemes on a mesh with 200 cells are shown in Figures 3.7. The $L_1$ numerical errors against the CPU time of different fluxes for different meshes are shown in Figure 3.8. In this case, the lines of the WENO-LF scheme, the WENO-LLF scheme and the WENO-FORCE scheme keep in bottom layer, while the WENO-HLLC scheme and the WENO-HLL scheme stay in top layer.

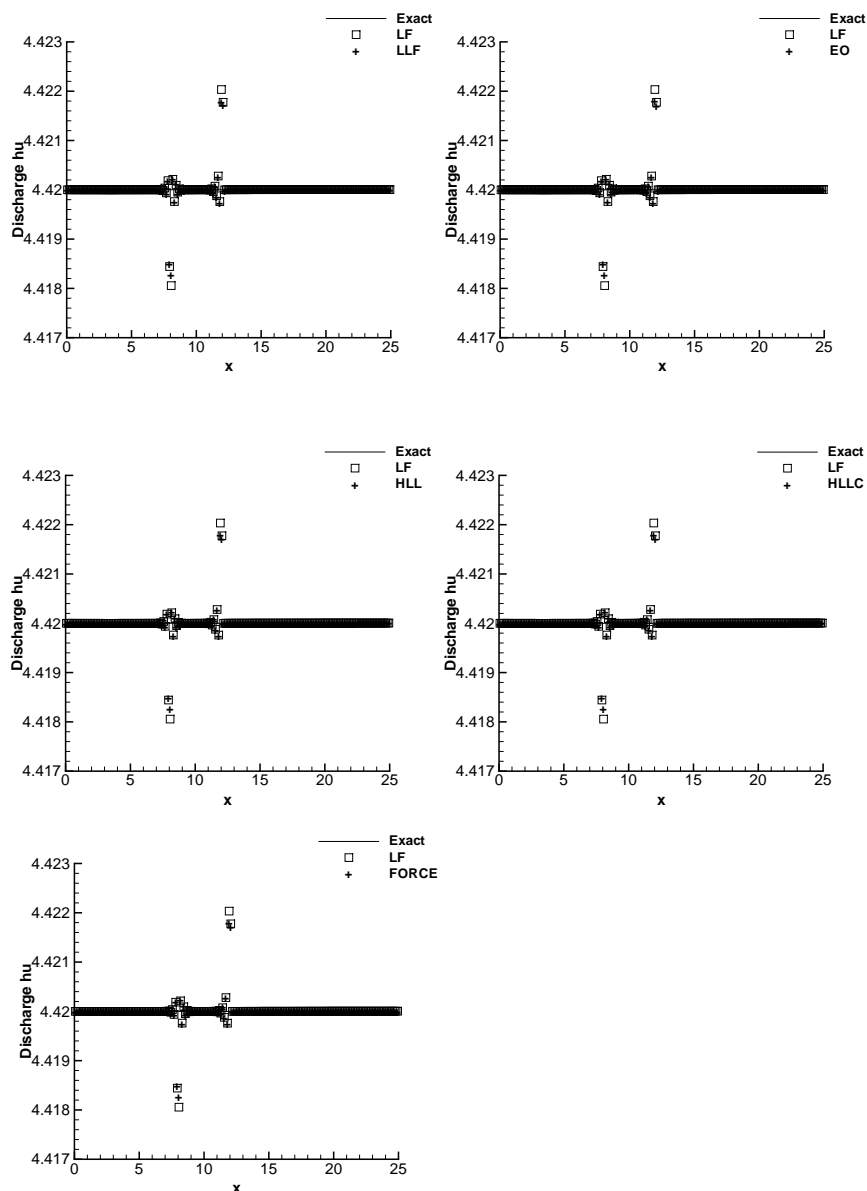From the results, we also can see that the results using the WENO-EO, WENO-HLL,

Fig. 3.7. Steady sub-critical flow over a hump. The discharge $hu$. Solid lines: the exact solution; hollow square: the results computed by the WENO-LF scheme; plus symbols: results computed by the WENO-LLF (top left), WENO-EO (top right), WENO-HLL (middle left), WENO-HLLC (middle right), and WENO-FORCE (bottom).

WENO-HLLC schemes are better for these situations. The numerical errors computed by the WENO-LLF are almost the same as that of the WENO-LF scheme for the discharge. On the test case (a), the numerical results computed by the WENO-EO, WENO-HLL, WENO-HLLC schemes are better than that by the WENO-LF scheme, while small difference between the results of those schemes and that of the WENO-LF scheme on the test case (b) is observed.
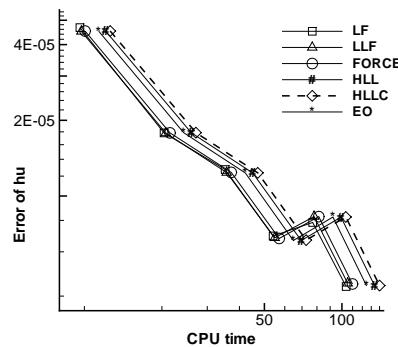
Fig. 3.8. Steady sub-critical flow over a hump. The $L_1$ numerical error for $hu$ and the CPU time (unit: second) using the log scale by the WENO methods based on different numerical fluxes on meshes with $N = 200, 300, 400, 500, 600, 700$ cells .

**Example 3.4.** Pulse over a hump [12, 17, 27]. We compute the solutions obtained when a small perturbation of the initially still water arises. In this way we test whether the numerical schemes obtain the correct wave speed propagation. The bottom elevation is described by the following function:

$$b(x) = \begin{cases} 0.25(\cos(10\pi(x - 1.5)) + 1) & 1.4 \leq x \leq 1.6, \\ 0 & \text{otherwise,} \end{cases} \tag{3.9}$$

where $x \in [0, 2]$. The initial conditions are taken as:

$$h(x, 0) = \begin{cases} 1 - b(x) + \beta & 1.1 \leq x \leq 1.2, \\ 1 - b(x) & \text{otherwise,} \end{cases} \quad hu(x, 0) = 0. \tag{3.10}$$

The duration of the simulation is 0.2s for the small pulse $\beta = 0.001$. For this small pulse problem, we take the small constant in the WENO weight formula $\varepsilon = 10^{-12}$, such that it is smaller than the square of the perturbation. We take the still level $D$ as $D(x) = 1 - b(x)$.

The initial disturbance is split in two waves. The left-going wave leaves the domain undisturbed. The right-going wave interacts with the hump.

In Figures 3.9-3.10, the computed surface level $h + b$ and discharge $hu$ with 200 uniform cells are plotted against the reference solution computed by WENO-LF with 3000 cells and against the numerical solution computed by the WENO-LF scheme on the same mesh. We can see that the results computed by the WENO-LF, WENO-EO, WENO-HLL and WENO-HLLC are comparable, and an overall good behavior of these schemes is shown. This demonstrates the good balancing between source term and flux gradient in unsteady problems.

**Example 3.5.** Asymmetric breaks of a dam. We consider the sudden break of a dam separating two basins with heights $5m$ and $10m$ in the two-dimensional shallow water equations. The length of the breach is $75m$ and it starts at $y = 95m$. The dam is positioned at $x = 100m$. The dam breaks asymmetrically at $t = 0$ and we simulate the problem until time $t = 7.2s$. Reflective boundary conditions are applied on all the edges of the domain. The test was used in [4, 17, 22].

We show the results obtained by the WENO schemes with different numerical fluxes in Figure 3.11 in terms of surface level contours on the same unstructured meshes with 17658 cells, the details of the WENO scheme on unstructured meshes see in [9]. The contour plots
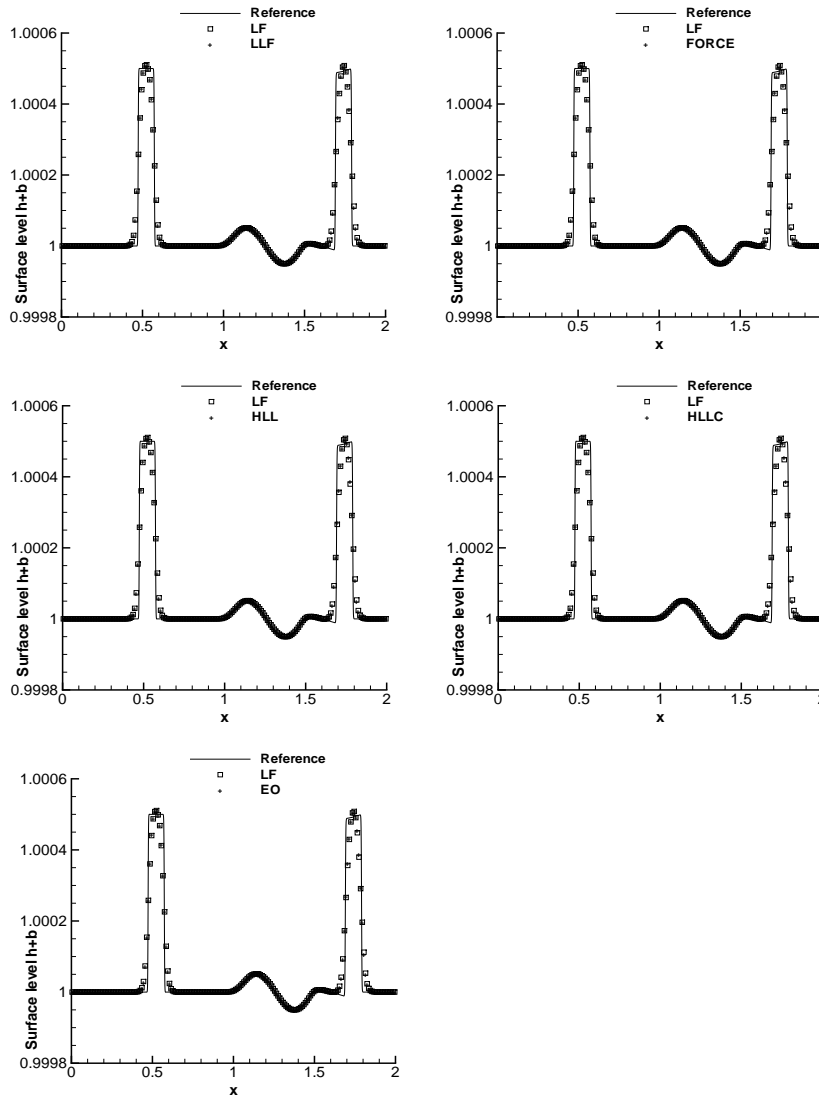
Fig. 3.9. Pulse over a hump. The surface level $h + b$. Solid lines: the reference solution; hollow square: the results computed by the WENO-LF scheme; plus symbols: the results computed by the WENO-LLF (top left), WENO-FORCE (top right), WENO-HLL (middle left), WENO-HLLC (middle right), and WENO-EO (bottom).

show that these schemes compute in a very smooth way the water acceleration on the left of the dam, while the water wave moving to the right is very sharp and monotone in all of the results. The reflection of this wave on the upper wall of the domain is clearly visible.

In Table 3.2, the CPU time comparison is reported. On the CPU time, almost the same conclusion of the one-dimensional case is got except that the WENO-EO scheme costs a little more CPU time than the WENO-HLLC scheme, while the WENO-HLLC scheme costs a little more CPU time than the WENO-EO scheme in one-dimensional case, as there are more states for the WENO-EO scheme in two-dimensional case.
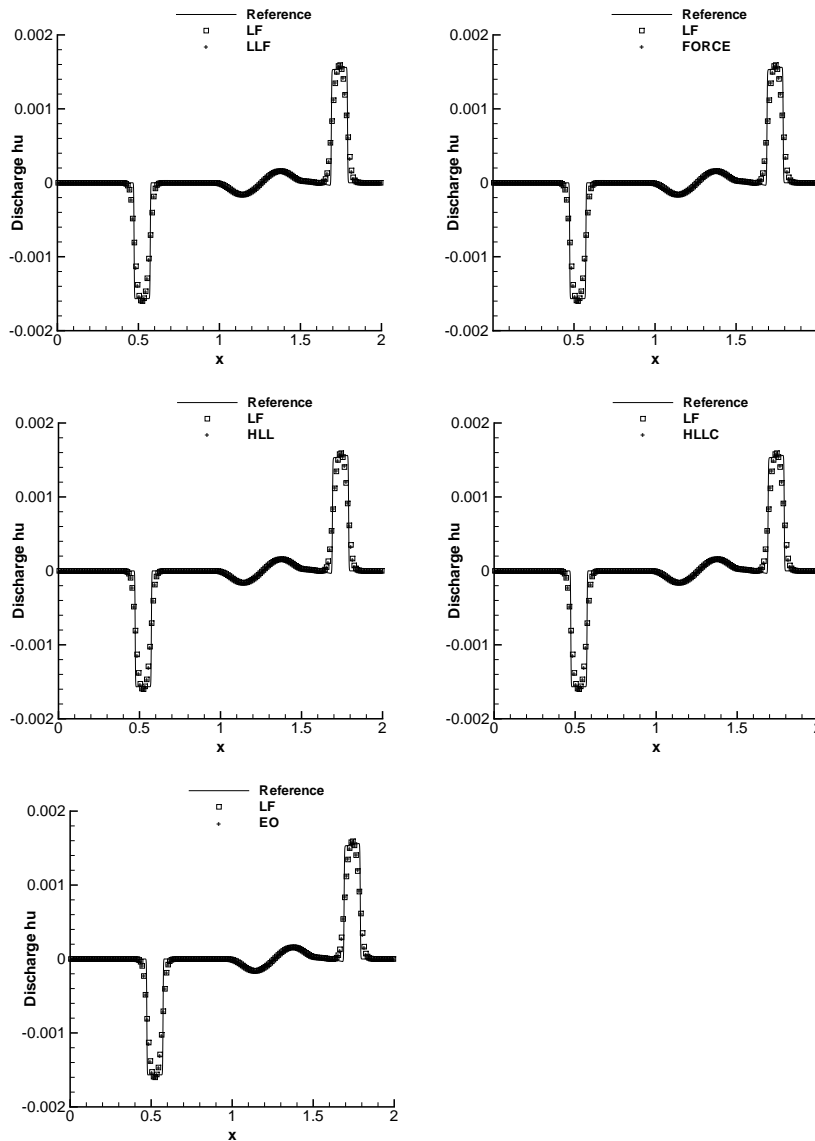
Fig. 3.10. Pulse over a hump. The discharge $hu$. Solid lines: the reference solution; hollow square: the results computed by the WENO-LF scheme; plus symbols: the results computed by the WENO-LLF (top left), WENO-FORCE (top right), WENO-HLL (middle left), WENO-HLLC (middle right), and WENO-EO (bottom).

**Example 3.6.** Trans-critical breaks of a circular dam. We simulate the break of a circular dam [8, 19] separating with water levels $10m$ and $1m$. The radius of the initial discontinuity is $r = 22$. Due to the difference in water height, the flow becomes rapidly trans-critical. This is an axially symmetric flow; we divide the domain with regular triangle meshes to keep the symmetry. Reflective boundary conditions are applied on all the edges of the domain. The simulations have been run using the WENO schemes with different numerical fluxes until time $t = 0.69s$. The comparisons of the surface level distributing along the line $y = 25$ from $x = 25$
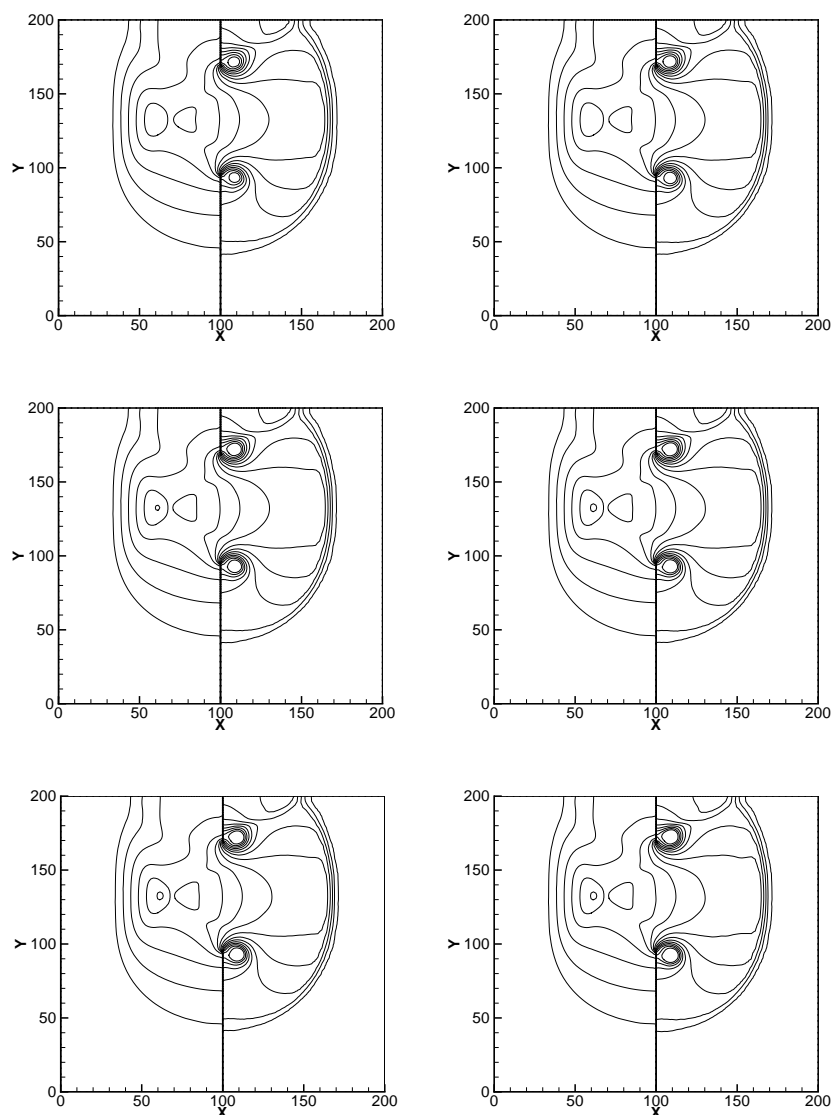
Fig. 3.11. Asymmetric break of a dam. Surface level contours at time $t = 7.2s$. 15 contours between 4 and 9.5. The WENO-LF (top left), WENO-LLF (top right), WENO-FORCE (middle left), WENO-HLL (middle right), WENO-HLLC (bottom left), and WENO-EO (bottom right).

to $x = 50$ using the WENO-LF scheme with the other schemes are reported in Figure 3.12. The numerical solutions obtained on a mesh of 1m-longth-sides cells; the reference solution obtained on a mesh of $\frac{1}{8}m$-length-sides cells.

We can see from the figures that the numerical results using the WENO-EO, WENO-HLL, WENO-HLLC schemes fit the reference solution better than those by the WENO-LLF, WENO-FORCE and WENO-LF schemes.
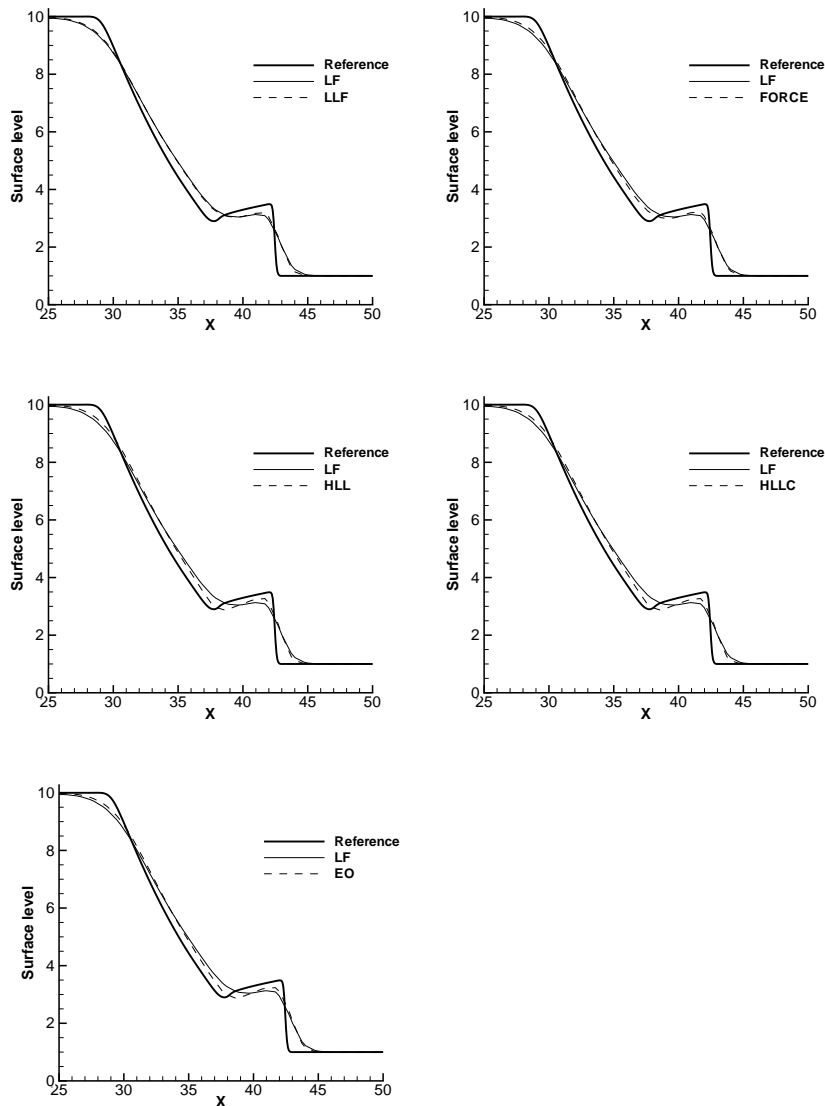
Fig. 3.12. Trans-critical break of a circular dam at $t = 0.69s$. The surface level distributing along the line $y = 25$ from $x = 25$ to $x = 50$. Heavy solid lines: the reference solution; Solid lines: the results computed by the WENO-LF scheme; Dashed line: the results computed by the WENO-LLF (top left), WENO-FORCE (top right), WENO-HLL (middle left), WENO-HLLC (middle right), and WENO-EO (bottom).

## 4. Concluding Remarks

In this paper, we have studied a few numerical fluxes for the WENO schemes for the one-dimensional and two-dimensional shallow water flows. The numerical results indicate that the WENO-LF scheme costs the least CPU time, but the numerical errors and resolution of solutions on the discontinuities are the worst among all. The WENO-LLF and WENO-FORCE schemes

Table 3.2: Asymmetric break of a dam. CPU time on the unstructured meshes using the WENO methods based on different fluxes (unit: second).

|          | LF   | LLF  | FORCE | HLL   | HLLC  | EO    |
| -------- | ---- | ---- | ----- | ----- | ----- | ----- |
| CPU time | 83.9 | 86.3 | 100.5 | 106.0 | 110.4 | 121.6 |

cost a little more CPU time and have a little goodness on errors than that of the WENO-LF scheme. The WENO-HLL, WENO-HLLC and WENO-EO schemes cost more CPU time than the WENO-LF scheme, while the WENO-HLL and WENO-HLLC schemes cost a little more than the WENO-EO scheme for the one-dimensional cases. However, the WENO-EO scheme costs the most hereinto for the two-dimensional cases. The cost time by the WENO-HLL, WENO-HLLC and WENO-EO schemes is worthy for the great resolution of solutions on the discontinuities and less errors than the WENO-LF scheme especially for the tests with shocks and discontinuities. As a result, the HLL, HLLC and EO numerical fluxes are good choices as the numerical fluxes with the WENO schemes for the shallow water equations.

# References

[1] K. Anastasiou and C.T. Chan, Solution of the 2D shallow water equations using the finite volume method on unstructured triangular meshes, *Int. J. Numer. Meth. Fl.*, **24** (1997), 1225-1245.

[2] C. Berthon, P. Charrier and B. Dubroca, An HLLC scheme to solve the M1 model of radiative transfer in two space dimensions, *J. Sci. Comput.*, **31** (2007), 347-389.

[3] V. Caleffi, A. Valiani and A. Bernini, Fourth-order balanced source term treatment in central WENO schemes for shallow water equations, *J. Comput. Phys.*, **218** (2006), 228-245.

[4] V. Caleffi, A. Valaini and A. Zanni, Finite volume method for simulating extreme flood events in natural channels, *J. Hydraul. Res.*, **41** (2003), 167-177.

[5] N. Črnjarić-Žic and S. Vuković, Balanced finite volume WENO and central WENO schemes for the shallow water and the open-channel flow equations, *J. Comput. Phys.*, **200** (2004), 512-548.

[6] O. Friedrichs, Weighted essentially non-oscillatory schemes for the interpolation of mean values on unstructured grids, *J. Comput. Phys.*, **144** (1998), 194-212.

[7] S.K. Godunov, Finite difference methods for the computation of discontinuous solutions of the equations of fluid dynamics, *Math. Sbornik.*, **47** (1959), 271-306.

[8] V. Guinot, An approximate two-dimensional Riemann solver for hyperbolic systems of conservation laws, *J. Comput. Phys.*, **205** (2005), 292-314.

[9] C.Q. Hu and C.W. Shu, Weighted essentially non-oscillatory schemes on triangular meshes, *J. Comput. Phys.*, **150** (1999), 97-127.

[10] G.S. Jiang and C.W. Shu, Efficient implementation of weighted ENO schemes, *J. Comput. Phys.*, **126** (1996), 202-228.

[11] E. Johnsen and T. Colonius, Implementation of WENO schemes in compressible multicomponent flow problems, *J. Comput. Phys.*, **219** (2006), 715-732.

[12] R.J. LeVeque, Balancing source terms and flux gradients in high-resolution Godnuov methods: the quasi-steady wave propagation algorithm, *J. Comput. Phys.*, **146** (1998), 346-365.

[13] R.J. LeVeque, Finite Volume Methods for Hyperbolic Problems, *Cambridge, University Press*, (2002).

[14] X.D. Liu, S. Osher and T. Chan, Weighted essentially non-oscillatory schemes, *J. Comput. Phys.*, **115**(1994), 200-212.

[15] A. Mohammadian, D.Y. Le Roux and M. Tajrishi, A conservative extension of the method of characteristics for 1-D shallow flows, *Appl. Math. Model*, **31** (2007), 332-348.

[16] K.W. Morton and P.K. Sweby, A comparison of flux limited difference methods and characteristic Galerkin methods for shock modelling, *J. Comput. Phys.*, **73** (1987), 203-230.

[17] S. Noelle, N. Pankratz, G. Puppo and J.R. Natvig, Well-balanced finite volume schemes of arbitrary order of accuracy for shallow water flows, *J. Comput. Phys.*, **213** (2006), 474-499.

[18] J. Qiu, B.C. Khoo and C.W. Shu, A numerical study for the performance of the Runge-Kutta discontinuous Galerkin method based on different numerical fluxes, *J. Comput. Phys.*, **212** (2006) 540-565.

[19] M. Ricchiuto, R. Abgrall and H. Deconinck, Application of conservative residual distribution schemes to the solution of the shallow water equations on unstructured meshes, *J. Comput. Phys.*, **222** (2007), 287-331.

[20] B.D. Rogers, A. G. L. Borthwick and P. H. Taylor, Mathematical balancing of flux gradient and source terms prior to using Roe's approximate Riemann solver, *J. Comput. Phys.*, **192** (2003), 422-451.

[21] C.W. Shu, Essentially Non-Oscillatory and Weighted Essentially Non-Oscillatory Schemes for Hyperbolic Conservation Laws, *ICASE Report No. 97-65*, (1997), 1-79.

[22] J.J. Stoker, Water Waves, *New York, Wiley-Interscience*, (1957).

[23] E.F. Toro, Riemann Solvers and Numerical Methods for Fluid Dynamics, A Practical Introduction, *Springer, Berlin,* (1997).

[24] E.F. Toro, Shock Capturing Methods for Free Surface Shallow Flows, *Chichester*, (2001).

[25] E.F. Toro, M. Spruce and W. Spears, Restoration of the contact surface in the HLL-Riemann solver, *Shock waves*, **4** (1999), 25-34.

[26] S. Vukovic and L. Sopta, ENO and WENO Schemes with the Exact Conservation Property for One-Dimensional Shallow Water Equations, *J. Comput. Phys.* , 179(2002), 593-621.

[27] Y.L. Xing and C.W. Shu, High order well-balanced finite volume WENO schemes and discontinuous Galerkin methods for a class of hyperbolic systems with source terms, *J. Comput. Phys.*, **214** (2006), 567-598.